Desalination and Water Treatment
www.deswater.com

doi: 10.5004/dwt.2021.26677

213 (2021) 248–258
February

Enhanced bromate adsorption by using α-FeOOH pillared bentonite

Cheng Zhong[a,†], Rui Deng[b,*,†], Meng Gao[a], Yunpeng Cao[b], Pan Weiliang[b], Li Gu[a,*], Qiang He[a]

[a]*Key laboratory of the Three Gorges Reservoir Region's Eco-Environments, Ministry of Education, Institute of Environment and Ecology, Chongqing University, 174 Shapingba Road, Chongqing 400045, China, emails: guli@cqu.edu.cn (L. Gu), 605749178@qq.com (C. Zhong), 3297245942@qq.com (M. Gao), heqiang@cqu.edu.cn (Q. He)*
[b]*School of Architecture and Urban Planning, Chongqing Jiaotong University, 66 Xuefu Avenue, Chongqing 400074, China, emails: 21260091@qq.com (R. Deng), 824143586@qq.com (Y. Cao), pan0316@126.com (P. Weiliang)*

Received 18 April 2020; Accepted 14 October 2020

ABSTRACT

Bromate is a toxic substance in water. This paper attempts to adsorb bromate by using ferric hydroxide pillared bentonite (α-FeOOH bentonite). The research compares the adsorbability among Na-bentonite, Fe pillared bentonite, and α-FeOOH bentonite, while the results indicated that the α-FeOOH bentonite presented higher efficiency in adsorption of bromate. The effects of different supporting ratios of α-FeOOH on bentonite were also conducted and the results indicated that 8% is the best supporting ratio. Based on this supporting ratio, the theoretic maximum adsorption capacity of the α-FeOOH bentonite reached 19.56 mg/g. The results kinetics study revealed that the adsorption process can well be described by the pseudo-second-order kinetics. The bromate in solution was rapidly removed/adsorbed during the first 10 min, and then the adsorption slowed down and tended to attain an equilibrium within later 50 min. The solution's pH determined the adsorptive performances, and the acidic pH condition was much more favored. Impacts of different competing anions and natural organic matters were conducted and they all presented some negative effects on the adsorption process. The results of our study indicated that the α-FeOOH bentonite presents great potential impacts on adsorption of bromate from water.

Keywords: Bromate; α-FeOOH-pillared bentonite; Enhanced adsorption

1. Introduction

In recent years, bromate is receiving more concerns due to the increased worries about disinfection by-products in potable water. Bromate is formed in the ozone disinfection of bromide (Br^-) contained water [1,2], and it has been classified as a carcinogenic substance to humans by the United States Environmental Protection Agency (USEPA). It is reported that bromate can cause the symptom of vomiting, nausea, and abdominal pain [3,4]. Because of the toxicities of bromate, a maximum limit of the concentration of 10 μg/L has been set by the World Health Organization (WHO), the European Commission, and USEPA [5]. Therefore, it is urgent to pursuit effective methods to remove it from water.

Servals methods, including electrocatalytic reduction [6], zero-valent iron reduction [7,8], ion exchange [9,10], and membrane filtration [11], have been introduced during the past decades. However, there are still some limitations to them in practical application due to their complicated procedure and their high operational costs. Comparatively,

* Corresponding authors.

† These authors have contributed equally to this work.

adsorption derived processes, which are quite simple in design and without harmful by-products formation during treatment, seem to be more attractive. In the field of water treatment, activated carbon is used widely, but it is commonly applied in adsorption of organic substances in solution or gas [12,13]. Owing to the high cost or low adsorption performance of adsorbent materials in literature, researches have been continued to explore inexpensive alternative adsorbents that high reasonably adsorption efficiencies [14]. Hence, there has been growing interest in seeking alternatives. According to previous studies, mineral-based cheap adsorbent, such as bentonite, zeolite, kaolin, etc., are now attracting more attention in water treatment [15–17].

Bentonite is a typical clay mineral, which has been widely used in the industrial field [18]. The unit layer structure of bentonite consists of one $A1^{3+}$ octahedral sheet placed between two Si^{4+} tetrahedral sheets. Under the effect of isomorphous substitution of Al^{3+} for Si^{4+} in the tetrahedral layer and Mg^{2+} for Al^{3+} in the octahedral layer, the bentonite is commonly negatively charged. The permanent charge on bentonite can be offset by different kinds of cations such as Na^{+}, Ca^{2+}, as well as some inorganic hydroxyl-metal polycations. The irreversible fixation of these kinds of polycations into bentonite's layers resulted in modified bentonite, named as pillared bentonite [19–21]. Bentonite is of great importance in industrial applications due to its good adsorptive, rheological, and catalytic properties [22]. In the period of the past decades, several hydroxyl-metal polycations including Al, Fe, Ti, Zn, etc., have been introduced and tested [23–26]. Hydroxy-aluminum and hydroxy-ferric polycations are most frequently introduced and tested. These pillared bentonites have been applied to adsorb metals, dyes, and other pollutants [27,28]. It is acknowledged [29] that iron and aluminum oxides play an important role in the removal of anions from aqueous solutions. Granular ferric hydroxide (GFH) has been developed and applied successfully for adsorbing arsenic, fluoride, as well as natural organic matters (NOMs) to remove them from solution, and it shows good performance in adsorption.

In the pillaring process, ferric hydroxide or aluminum hydroxide can easily be inserted into the inner layers of bentonite structure and the interlayer distance of the bentonite can obviously be increased. The introduction of these preferably inorganic pillars not only provided specific functional groups but also increases micro-porosity of the materials, which would induce a greater surface area and result in an improvement in material's resistance and stability. Hence, the ferric hydroxide pillared bentonite is expected to have higher adsorption capacities towards bromate. However, up to now, the research about bromate removal by ferric hydroxide pillared bentonite adsorption is still limited.

Accordingly, this paper tries to remove bromate through the method of adsorption by using ferric hydroxide pillared bentonite. The ferric hydroxide pillared bentonite was prepared and characterized. The equilibrium and kinetic studies were performed, aiming to have a better description of the adsorption process. The impacts of different adsorption parameters such as initial bromate concentration, contact time, pH, as well as the competing anions are examined. Different adsorption isotherms and kinetic models are discussed.

2. Materials and methods

2.1. Chemicals and materials

Natural bentonite, which is composed primarily of Ca^{2+}-montmorillonite, was obtained from Lin'an, Zhejiang Province, China. Its cation exchange capacity is about 90.4 mmol/100 g. Bromate stock solution (1 g/L) was firstly prepared by dissolving $KBrO_3$ (Sinopharm Chemical Reagent Co., Ltd., China) into deionized water. The dilutions with different concentrations (2–250 mg/L) were then prepared according to this stock solution. All selected chemicals in this study were analytical reagent grade. Solution pH was adjusted by adding HCl and NaOH with their concentration of 0.1 M.

2.2. Preparation of pillared bentonite (Fe-B)

The α-FeOOH-pillared bentonite was prepared through the hydrolyzing process of hydroxyl-Fe-pillared bentonite in alkaline solution' whose preparing procedure can be found in the literature [30]. Through adding NaOH, the pH of the solution containing specific amounts of hydroxyl-Fe-pillared bentonite was adjusted to 12.0. Then the slurry was aged at 75°C with violent stirring for 1 week. Then, the bentonite in solution was filtered and washed. Finally, the product was dried at 55°C and ground and sieved through a 200-mesh screen. The procedure of the preparation is shown in Fig. 1.

2.3. Adsorption experiments

2.3.1. Bromate adsorption kinetics

Bromate adsorption kinetics was evaluated for α-FeOOH bentonite. Before the start of the kinetic experiment, approximately 0.2 g of the sample was loaded in a 500 mL conical flask. Then, 500 mL of solution with different bromate concentrations (2.0, 5.0, 10.0, 20.0, 30.0, 50.0, and 100.0 mg/L) was added. The pH of the solution was maintained at 7.0 ± 0.1 by adding either 0.1 N HCl or 0.1 N NaOH stock solutions. The flask was capped and immediately immersed in a thermostatic shaker bath at 25°C with the shaking speed of 200 rpm. Then samples were taken out from the flask at different time intervals from 0 to 4 h of adsorption and filtered through a 0.45 μm membrane before analysis.

2.3.2. Isotherm studies

The equilibrium batch experiments were carried out to investigate the adsorption capacity of the bentonite with different loading ratios of α-FeOOH. In this experimental section, a series of conical flasks containing 500 mL solution with the bromate concentrations in the range of 0–200 mg /L were prepared. Approximately 0.2 g of the samples with different loading ratios of α-FeOOH (2%, 5%, 8%, and 15%) were added into the flasks. The pH of the solution was maintained at 7.0 ± 0.1. Each flask was capped and shaked for 48 h to ensure attaining approximate equilibrium. Then the supernatants were taken for analysis.

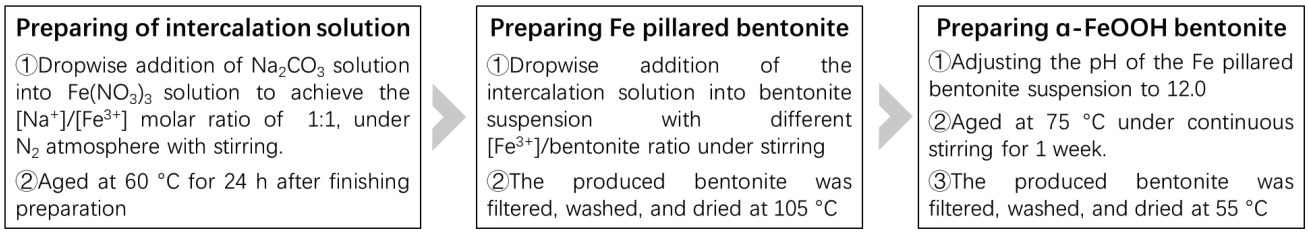

Fig. 1. Preparing procedure of α-FeOOH bentonite.

2.3.3. Effects of various experimental parameters

The effect of pH, NOM, and competing anions on the adsorption was carried out. In this section, 0.2 g of the sample was added into the conical flask containing 500 mL solution with the bromate concentration of 30 mg/L. pH was adjusted to 3.0, 5.0, 7.0, 9.0, 10.0, and 11.0 to understand its effects. The effect of NOM was carried out by adding different amounts of NOM (simulated by humic acid, 0.5, 1.0, 2.0, 4.0, 8.0, and 15.0 mg/L) into the solution. Different kinds of anions including chloride, sulfate, nitrate, and bromide with the concentrations of 0.25, 0.50, 0.75, 1.0, 1.25, and 1.50 mmol/L in the solution were prepared to understand the effect of the anions on adsorption. The adsorption process finished in 4 h and then the supernatants suppressed conductivity detector was maintained at 35°C ± 0.1°C. The bromate concentrations were measured two times, and the mean values were applied.

Specific surface area, total pore volume, and average pore size of different samples were determined from the N_2 adsorption data at 77 K. The equilibrium nitrogen adsorption at 77 K was measured using by Micromeritics, ASAP2020M+C, USA. All the samples were firstly degassed at 623 K for 2 h and then proceed to test. The specific surface areas of the samples were determined by applying the Brunauer–Emmett–Teller (BET) equation to the measured data. The total pore volume was determined using the Brunauer MP method [31]. The average pore size can be calculated by dividing the pore volume by the specific surface area.

Fourier transform infrared (FTIR) experiments were carried out on a spectrometer (Nicolet, IS10, USA). The bentonite powders were mixed with KBr solid, respectively. The mixed powders were pressed to tablets with 1 cm in diameter. Then the tablets were inserted into the apparatus and the spectra were recorded from 4,000 to 400 cm^{-1}.

X-ray powder diffraction (XRD) measurements of the α-FeOOH-bentonite were carried out using Siemens (Germany) X-ray diffractometer D5005 (Cu Kα radiation, $2\theta = 5°–60°$).

3. Result and discussion

3.1. Surficial properties of different materials

3.1.1. Porous structure parameters for different bentonites

Nitrogen adsorption–desorption process is conducted for different bentonites to reveal their porous structures. Na-bentonite, before pillaring, as well as Fe pillared bentonite, which is frequently applied in adsorption anions, were adopted to provide a comparison with α-FeOOH bentonite. N_2 adsorption/desorption isotherms for different samples are presented in Fig. 2. It can be seen from Fig. 2, that for the tested samples, almost all of the N_2 adsorption isotherms can be categorized as type IV of the IUPAC classification (typical macroporous adsorbent). Main porous properties including BET specific surface area, average pore radius (R_p), and pore volume (V_p), which can be obtained from the N_2 isotherms results, are also presented in Table 1.

From Table 1, the specific BET surface area (S_{BET}) of the Na-bentonite is about 21.3 m^2/g with the pore volume (V_p) of 0.039 cm^3/g. The pillaring process changes the porous structures, and the S_{BET} of the Fe pillared bentonite with the Fe/OH ratio of 1/1 increases to 77.6 m^2/g, which is about 3.3 times that of the Na-bentonite. The pore volume is also increased from 0.05 to 0.21 cm^3/g in the pillaring process. The α-FeOOH-bentonite presents a richer pore structure, and its BET surface is about 113.2 m^2/g, which is about 45.9% higher than that of the Fe pillared bentonite. The pore size distribution of α-FeOOH-bentonite according to Barrett–Joyner–Halenda [31] presented a maximum for the distribution at a pore radius of 4.82 nm. The increase of the specific BET surface area and pore volume indicates that the pillaring process presents a positive effect on the porous structure of the bentonite, and the form of α-FeOOH crystal in the interspaces can further increase the porous structure. The insertion of pillars and promotion in porous structures are expected to cause some increases on the adsorption ability toward anions. However, the specific surface area in this study is much lower than that of commercial GFH, whose BET surface is about 206 m^2/g with a pore volume of 0.76 cm^3/g. The GFH has been adopted in As(V) and bromate adsorption, the performance of the GFH is applied to give a comparison with the α-FeOOH-bentonite [29,32].

3.1.2. FTIR spectra

FTIR spectra of the Na-bentonite, Fe pillared bentonite, and α-FeOOH pillared bentonite are given in Fig. 3. The bending peaks are mainly concentrated in the ranges of 4,000–3,000 cm^{-1} and 2,000–400 cm^{-1}. The peaks between the regions of 3,550 and 4,000 cm^{-1} commonly represented to the structural hydroxyl groups, sometimes these peaks may also be aroused by the water molecules in the interlayer. The intensity of these peaks increased slightly under the effect of the pillaring process. The peaks centered at about 1,050 cm^{-1} in the spectra represented the Si–O–Si stretch, and it can also be noticed that there is a rare change in the intensity of this peak. The peaks at 523 and 796 cm^{-1} are considered as Al–O–Si deformation and Si–O

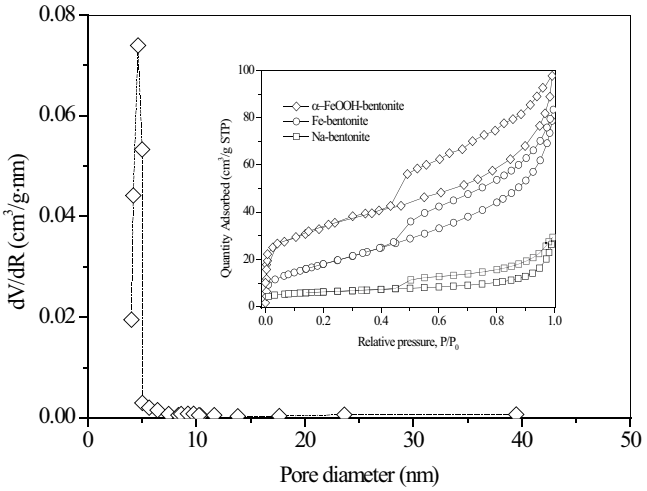

Fig. 2. N_2 adsorption/desorption isotherms and pore size distributions for different samples.

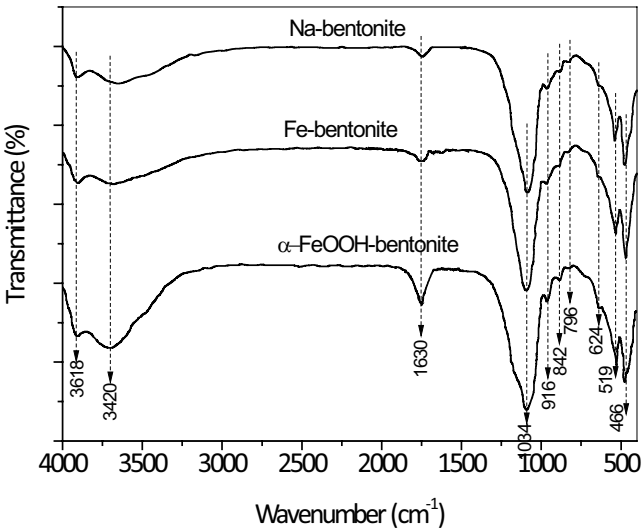

Fig. 3. FTIR spectra of different materials.

Table 1
Textural property of bentonite sample

Samples	BET specific surface area (m^2/g)	Total pore volume (cm^3/g)	Average pore size (nm)
Na-bentonite	21.3	0.039	3.68
Fe-bentonite	77.6	0.21	4.99
α-FeOOH bentonite	113.2	0.23	5.23

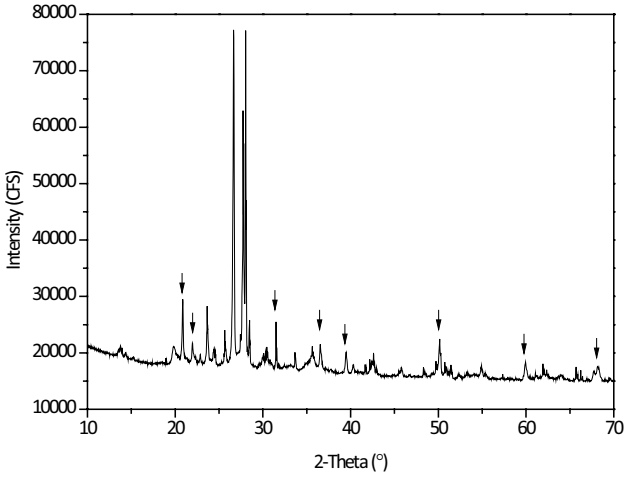

Fig. 4. XRD data for α-FeOOH bentonite.

stretching [30,31]. It can be found in the Fig. 3 that there was a decline in the peak intensity related to Al–O–Si deformation, which is brought by the pillaring process. However, there is no change in Si–O stretching. The Fe–O–Fe and Fe–O asymmetric stretching can hardly be clearly identified due to the frequently characteristic stretching of the virgin bentonite [12]. Overall, the modification process not only enlarges the surface area of the bentonite, but also brings plenty of surface functional groups on bentonite structure that is helpful in adsorption of anions.

3.1.3. X-ray diffraction

The crystalline structure of α-FeOOH-bentonite was identified by XRD measurements to ensure the successful preparation of the material. The XRD patterns obtained is shown in Fig. 4. The main diffraction peaks (2θ) centered at about 20.92°, 31.05°, 36.63°, 39.84°, 50.29°, and 59.88° can be attributed to the crystalline phase of α-FeOOH (goethite) [30]. The results indicated that the α-FeOOH-bentonite has been successfully prepared with good crystal structures.

3.2. Adsorbability of different materials

Comparison among different materials including Na-bentonite, Fe pillared bentonite, and α-FeOOH bentonite was conducted to understand the positive effect of the pillaring process of ferric hydroxide into the inner layer structures of the bentonite, and the results can be found in Fig. 5. Besides, the adsorption ability of commercial GFH reported in the literature is also referred here to provide a comparison. As can be seen from Fig. 5. The bromate uptake increases gradually with the increase of the equilibrium concentration, while the increase rate of the bromate uptake (q_m) slows down when the equilibrium concentration is higher than 100 mg/L. The Na-bentonite presents limited adsorption capacity for bromate uptake, while the pillaring process increases the adsorption capacities significantly. At the equilibrium concentration of about 200 mg/L, the adsorption capacity of the Fe pillared bentonite is about 8 mg/g while that for α-FeOOH bentonite is about 12 mg/g. The adsorption capacity of GFH reported in literature is about 15 mg/g under the same equilibrium concentration [29]. Though the adsorption capacity of Fe or α-FeOOH pillared bentonites is not as high as the commercial GFH, and the α-FeOOH pillared bentonite consumed less ferric element in their preparing (mass ratio for Fe to

bentonite was controlled at about 8%). These increase of the adsorption capacity brought by the pillaring process can be ascribed to the facts presented as follows: (1) compared to the virgin or Na-bentonite, the pillared bentonites including Fe and α-FeOOH pillared bentonites pose much higher specific surface area, resulting in the promotion of the contact opportunities between bromate anions and bentonite surface, (2) the pillared bentonites are reported to be less negatively charged than the Na-bentonite, and so there is a reduced repulsion force between the bentonite particles and the dissolved anions, and (3) according to previous studies, there is strong adsorption of dissolved substances onto the Al or Fe sites of the bentonite while limited adsorption occurs on the Si sites of bentonite. Therefore, the intercalation of Fe hydroxides into the structure of bentonite significantly promotes the adsorption capacity. Compared to the Fe pillared bentonite, the α-FeOOH bentonite presents much superiority in removing bromate, and so it is applied for subsequent kinetic and isothermal studies.

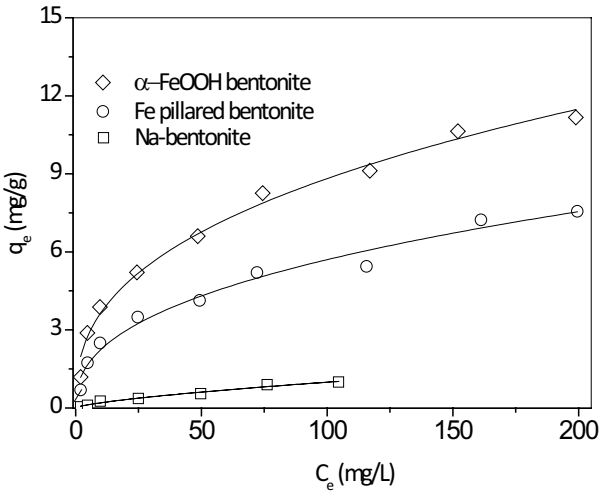

Fig. 5. Adsorption capability of different bentonites

3.3. Adsorption isotherm for bentonites supported by different amounts of ferric

To reveal the effect of supporting the ratio of ferric to bentonite, an adsorption isotherm study was carried out and the results can be seen in Fig. 6. The experimental isotherm data shown in Fig. 6 can be characterized by the typical *L*-curve isotherm, in which the initial slope remains relatively stable with the increase of the solute concentration. According to Fig. 6, the bromate uptake increases significantly with the increase of the equilibrium concentration from 0 to 30 mg/L. With the further increase of the equilibrium concentration, the increase of the bromate uptake slows down. Two types of isotherms including Langmuir and Freundlich [22,31], as described in Eqs. (1) and (2), are referred to fit the experimental data to descript the adsorption process.

Langmuir model:

$$q_e = \frac{q_m b C_e}{1 + b C_e} \tag{1}$$

Freundlich model:

$$q_e = K_f C_e^{1/n} \tag{2}$$

where C_e and q_e are the concentration (mg/L) in solution and the adsorbed amount (mg/g) of bromate when the adsorption equilibrium attains. q_m (mg/g) is the maximum monolayer adsorption capacity and b (L/mg) is a constant in Langmuir isothermal model related to the free energy of adsorption. K_f ($mg^{(1-n)}$ L^n/g) in the Freundlich model is the Freundlich constant related to the adsorption capacity, n is the energy or intensity of adsorption. These constants can also be determined by the regression of the isotherm data.

The calculated parameters for these models with the correlation coefficient (R^2) are shown in Table 2. It can be seen from the table that these adsorption data can be well-described by these models. In terms of the correlation coefficient R^2, the Langmuir isotherm model gives much

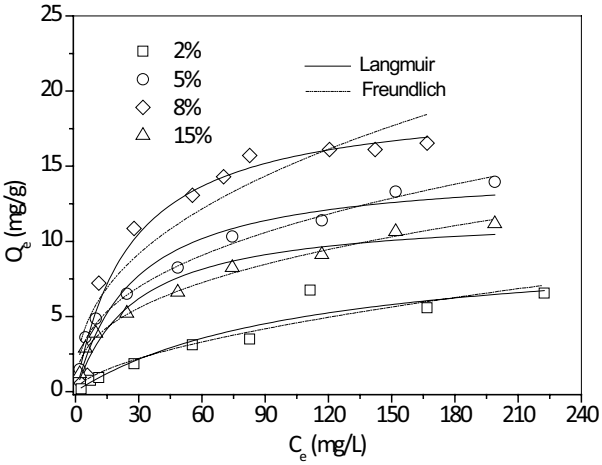

Fig. 6. Adsorption isotherms for α-FeOOH bentonite with different loading ratios.

better fitting results than that of the Freundlich model, indicating that the bromate was absorbed by monolayer adsorption with uniform energies and no transmigration of bromate occurred in the plane of the surface. The calculated parameters for these models give us a direct comparison of the adsorption capacity among different bentonites. The parameter q_m in the Langmuir equation commonly represents the theoretical maximum adsorption capacity of the tested adsorbent in adsorbing target pollutants. It can be seen from the table that the thermotical maximum adsorption capacity relies heavily on the loading amount of ferric on bentonite. With the increase in the loading amount from 2% to 8%, the maximum adsorption capacity was increased from 10.03 to 19.56 mg/g. Further increase in the loading amount to 15% brought a significant decline in maximum adsorption capacity to about 14.92 mg/g. The optimal ferric loading on bentonite should be 8%, and this kind of α-FeOOH was applied in a subsequent study. Similar isotherm results were reported for the adsorption isotherms of different pollutants by various

Table 2
Isotherm constants for bromate adsorption on α-FeOOH bentonite

Supporting ratios	Langmuir equation			Freundlich equation		
	q_m (mg/g)	b (L/mg)	R^2	K_F (mg$^{(1-n)}$ L^n/g)	n	R^2
2%	10.03	0.009	0.924	0.303	1.717	0.901
5%	11.92	0.0362	0.985	1.514	2.614	0.989
8%	19.56	0.0385	0.988	1.893	2.614	0.988
12%	14.92	0.0358	0.948	2.289	2.452	0.889

adsorbents [33,34]. These results indicate that the ferric hydroxide is the main active adsorption site on bentonite structure, and the more ferric hydroxide means larger amounts of the adsorption sites are available in adsorption. Also, it can be seen from Table S1 that there is a significant increase of the porous structure (specific surface area increased from 57.2 to 113.2 m^2/g) with the increase of the loading ratio from 2% to 8%. So, the increased porous structures of the bentonite may also be helpful for the adsorbability. Further increase of the supporting ratio brought blockage of the porous structure of bentonite (the specific surface area was decreased to 68.3 m^2/g, shown in Table S1), that hinders the entering of the bromate anion to the micro or mesopore in bentonite's structure, resulting in a significant declining of the maximum adsorption capacity.

3.4. Adsorption kinetics

3.4.1. Effect of contact time and initial bromate concentration

Effect of both contact time and initial bromate concentrations on bromate adsorption were investigated, and the results are shown in Fig. 7. It can be seen from the Fig. 7 that the bromate uptake increased rapidly during the first 15–25 min, and then the increase of the uptake slows down. From 50 to 250 min, there is little change in the bromate uptake. The results indicate that there is a fast adsorption of bromate at the early stage of the adsorption process, which is much faster than other adsorbents, such as powdered and granular activated carbons. They are reported to consume 0.5–1 h to reach equilibrium [33,34].

In addition, the adsorption process under different initial bromate concentrations was investigated, and the results are also shown in Fig. 7. It can be found in Fig. 7 that the bromate uptake relies heavily on the initial bromate concentrations, and higher uptake can be obtained when higher initial bromate concentration is adopted. The adsorbed amount at the end of the adsorption increased from 1.1 to 15.3 mg/g with the initial bromate concentration increased from 2 to 100 mg/L. This is quite normal in batch reactors due to the increased driving force of the concentration gradient at higher initial bromate concentrations [12].

3.4.2. Kinetic modeling

It is reported that kinetic modeling is one of the key paths in evaluating adsorption efficiency. Three different kinetic models including pseudo-first-order, Weber and Morris intraparticle diffusion model and Bangham's pore diffusion model have been applied here to further understand the adsorption mechanism of bromate on α-FeOOH bentonite. The fitting results of these models are discussed below and the calculated modeling parameters are provided in Table 3.

- *Pseudo-second-order model* [31]:

$$\frac{t}{q_t} = \frac{1}{k_1 q_e^2} + \frac{1}{q_e} t \tag{3}$$

where q_e and q_t are the amount adsorbed of bromate (mg/g) when equilibrium attains and the adsorption capacity at time t and k_1 is the rate constant for the pseudo-second-order kinetic (g/(min mg)). The plots between t/q_t vs. t were drawn in Fig. 7b. The results shown in this Fig. 7 indicates that there is a linear relationship between t and t/q_t. In literature, similar kinetic results were reported in the adsorption kinetic studies of some water pollutants onto adsorbent materials [35]. The slope and the intercept of plot can be used to determine the rate constants (k_1) and $q_{e,\mathrm{cal}}$ and they are list in Table 3 along with the correlation coefficient (R^2).

From the calculated correlation coefficients shown in Table 3, it is estimated that the data is well-fitted by the pseudo-second-order kinetic model. It can be seen from the table that the calculated adsorption rate constant k_1 is about 0.206 g/(min mg) when the initial bromate concentration is approximately 2 mg/L, indicating that there is a fast adsorption due the abundance of adsorbent in reaction compared to the target adsorbate. There is a steady decline of the rate constant with the increase of the initial concentration. The rate constant decreases from 0.147 to 0.014 g/(min mg) with the increase of the initial bromate concentration from 5 to 100 mg/L. The high values of the correlation coefficient (R^2), as well as the fact that theoretical $q_{e,\mathrm{cal}}$ fit well to the experimental data, indicates that the data can be defined favorably by the pseudo-second-order kinetic model.

- *Bangham's model*:

The Bangham model [17,31] is shown as following:

$$q_t = \frac{q_e - q_e}{\exp\left(kt^z\right)} \tag{4}$$

In this Eq. (4), the parameter k (1/min) is the adsorption rate constant in Bangham's model and z is a constant.

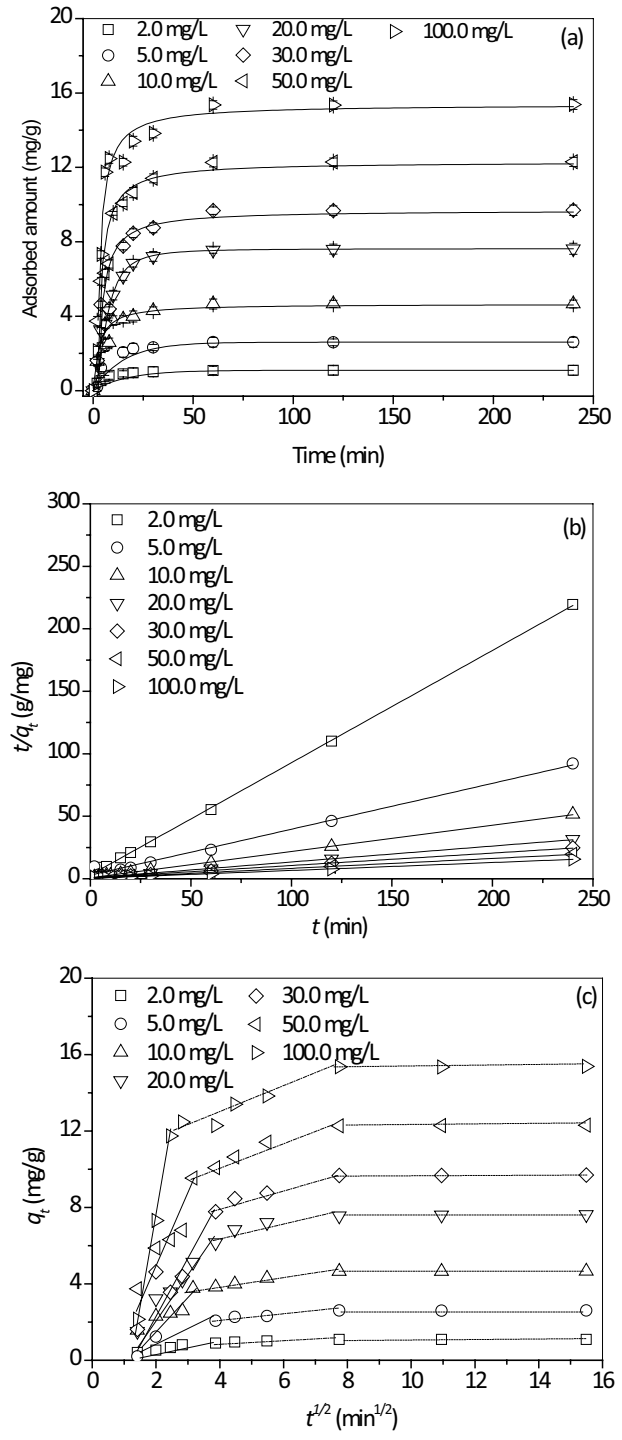

Fig. 7. Kinetic study for α-FeOOH adsorption: (a) effect of initial bromate concentrations; fitting results of the (b) pseudo-first-order kinetic model, and (c) Weber and Morris intra-particle diffusion model).

Table 3 shows the fitting curves and values of all parameters obtained by the fitting process. It can be seen from the table that the regression coefficients (R^2 values) of this model are excellent, and the theoretical q_e values are quite close to the real experimental data. So, the Bangham kinetics model could also be considered to describe the process of the bromate adsorption onto the bentonite. The fitting results reveal that the adsorption of bromate involved both the processes of surface adsorption and pore diffusion. The initial adsorption rate was relatively rapid, while the adsorption rate slowed down due to the occupation of the adsorption sites. Subsequently, anions tend to diffuse into inner pores to get a better contact with the adsorption sites hidden in bentonite porous structure, and the intraparticle diffusion may play a major role in subsequent adsorption. Thus, the rate of the adsorption process slowed down gradually until the equilibrium attained.

- Weber and Morris intraparticle diffusion model:

The transporting process of adsorbate in solution to adsorbent's surface can be divided into several phases. According to previous study, there are four mass transport mechanisms: diffusion at bulk space, film diffusion, intra-particle diffusion, and sorption into interior sites. It is commonly regarded that the film and intra-particle diffusion are the key steps that control the whole rate of adsorption due to the fact that the first and fourth steps are quite fast that they cannot limit the whole adsorption rate. Hence, the Weber and Morris intra-particle diffusion is commonly utilized to further understand on the diffusion mechanism during adsorption [12].

$$q_t = k_{\mathrm{id}} t^{1/2} + C \tag{5}$$

where k_{id} is the intra-particle diffusion rate constant (mg/g $\mathrm{min}^{1/2}$) and C (mg/g) is the constant, which is determined by the thickness of boundary layer. It is reported that the greater boundary layer effect commonly corresponds larger value of C.

When Weber and Morris plot of q_t vs. $t^{1/2}$ give straight line, it means that the adsorption process is controlled only by the intra-particle diffusion. If the data exhibit multi-linear plots, there are two or more stages influencing the adsorption process [12]. The Weber and Morris plots of bromate adsorption on α-FeOOH bentonite are also shown in Fig. 7c. In Fig. 7c, there are three straight lines in data points, indicating that the pore diffusion is not the unique rate-controlling step. It is assumed that in the early stages the external resistance is significant. In this phase, the bromate was adsorbed rapidly by the pillared bentonite through immediate utilizing the most readily available adsorption sites in the porous structures of the adsorbent. The second linear portion is the gradual adsorption stage with intra-particle diffusion dominating that the adsorbate diffusion from the surface into the inner pores slowly. The slope of the Weber and Morris plots are defined as the adsorption rate. The values of rate parameters ($k_{\mathrm{id},1}$ and $k_{\mathrm{id},2}$) can also be found in the table.

3.5. Effect of pH, NOM concentrations and competing anions on bromate sorption onto α-FeOOH bentonite

3.5.1. Effect of pH

pH is regarded as one of the key parameters which heavily influents the adsorbent efficiency. From Fig. 8a, the

Table 3
Rate constants and correlations coefficients for the studied kinetic models

C_0, mg/L	Pseudo-second-order model			Weber and Morris intra-particle diffusion model				Bangham's pore diffusion model			
	k_1, g/(min mg)	$q_{e,cal}$, mg/g	R^2	$k_{id,1}$, 1/min	R^2	$k_{id,2}$, 1/min	R^2	k, 1/min	q_e, mg/g	z	R^2
2	0.206	1.11	0.999	0.211	0.966	0.037	0.946	0.279	1.089	1.380	0.990
5	0.147	2.72	0.991	0.679	0.934	0.107	0.952	0.119	2.564	1.940	0.957
10	0.053	4.76	0.999	0.958	0.942	0.197	0.937	0.235	4.673	1.426	0.959
20	0.024	7.87	0.999	1.828	0.989	0.205	0.913	0.125	7.613	1.892	0.992
30	0.017	10.1	0.997	2.214	0.918	0.377	0.989	0.111	9.711	1.864	0.954
50	0.015	12.7	0.999	2.852	0.942	0.545	0.930	0.204	12.32	1.532	0.974
100	0.014	15.9	0.998	7.667	0.980	0.728	0.923	0.074	14.27	3.311	0.937

adsorption of bromate declines slowly with the increase of the pH, and the anions can hardly be adsorbed when pH is controlled higher than 10.0. In acidic pH conditions, (pH = 3.0–5.0), the adsorption capacity of the bentonite toward bromate was much higher than that in both neutral and alkaline pH conditions. At pH = 5.0–7.0, here occurs some declines in the adsorption capacity of the sorbent (near 1.0 mg/g). At pH = 7.0–10.0, a rapid decline of the adsorption capacity from 7.80 to 4.70 mg/g takes place. So, these results indicate that pH < 7.0 is the most favorable condition for bromate uptake due to the weak competition of OH^- anions. The adsorption of bromate depends on the charges of the bentonite surface. The pHzpc (pH at the point of zero charge) for the α-FeOOH bentonite is about 7.4–7.6. So, at pH conditions higher than 7.6, the bentonite surface tends to be negatively charged. Under the electrostatic repulsions between the bromate anions and the negatively charged surface, the adsorption capacities decline fast with the increase of the pH. The mechanism of bromate adsorption onto the α-FeOOH bentonite is quite accordant to that of anions adsorption on the metal oxide surface. In addition, the bentonite also participates in the adsorption process. The bromate adsorption by the metal oxides can be given as:

$$\equiv Fe-OH + BrO_3^- \leftrightharpoons \equiv Fe-BrO_3^- + OH^- \quad (6)$$

$$Fe(OH)^{2+}(aq) + BrO_3^- \leftrightharpoons (FeBrO_3)^{2+} + OH^- \quad (7)$$

A previous study [36] also confirmed that that the adsorption of anions on goethite mainly occurred by the coordination of anions to FeOH groups through below reaction:

$$FeOH^{-1/2} + H^+(aq) + BrO_3^-(aq) \leftrightharpoons FeBrO_3^{-1/2} + H_2O \quad (8)$$

In the adsorption process, the bromate interacts with coordinated FeOH groups and an exchange reaction against OH^- of surface groups appears [36]. In addition, the carrier bentonite also presents some positive effects on bromate adsorption by attracting bromate through the electrostatic force.

3.5.2. Effect of NOM concentration

It is well-known that NOM widely exists in natural water and wastewater, and could pose some influences on the adsorption process. So, in this study, effects of different NOM concentrations on bromate adsorption were carried out by using HA (humic acids) as a simulant, and the results are shown in Fig. 8b. As shown in Fig. 8, there is little change can be found in the bromate adsorption on the α-FeOOH bentonite in the NOM concentrations ranging from 1 to 5 mg/L in this study. The bromate uptake suffers a slight decline when the NOM concentrations is increased from 5 to 7.5 mg/L. Further increase of the NOM to 15 mg/L brings a significant decrease of the bromate uptake. In addition, it is worth note that the NOM in the solution can also be removed during the adsorption process, and the UV254 of the solution at the end of the reaction are lower than 0.01 cm^{-1} when the initial NOM concentration is lower than 7.5 mg/L. These results indicate that the adsorption capacity of the α-FeOOH bentonite is quite stable in bromate removal even in co-existing of NOM.

3.5.3. Effect of co-exist anions

There are other anions such as chloride, sulfate, etc., contained in water. Therefore, it is of great importance to understand the effect of these anions that may compete with bromate anion throughout the adsorption process. The adsorption study of bromate in presence of competing anions like bromine (Br^-), nitrate (NO_3^-), chloride (Cl^-), and sulfate (SO_4^{2-}) with different concentrations was carried out. The initial bromate concentration was set at about 20 mg/L. The results of these different competing anions effecting on bromate adsorption are shown in Fig. 8c. It can be observed from Fig. 8 that the competing anions presented different influence intensities on bromate adsorption. Little influence on bromate sorption was observed when chloride was present, due to the fact that it is one of outer-spherically sorbing anions, while significant effect is observed by anions of sulfate, nitrate, and bromide. This decrease in the bromate removal efficiency can be ascribed to the competition of anions for active sites in the structure of α-FeOOH bentonite.

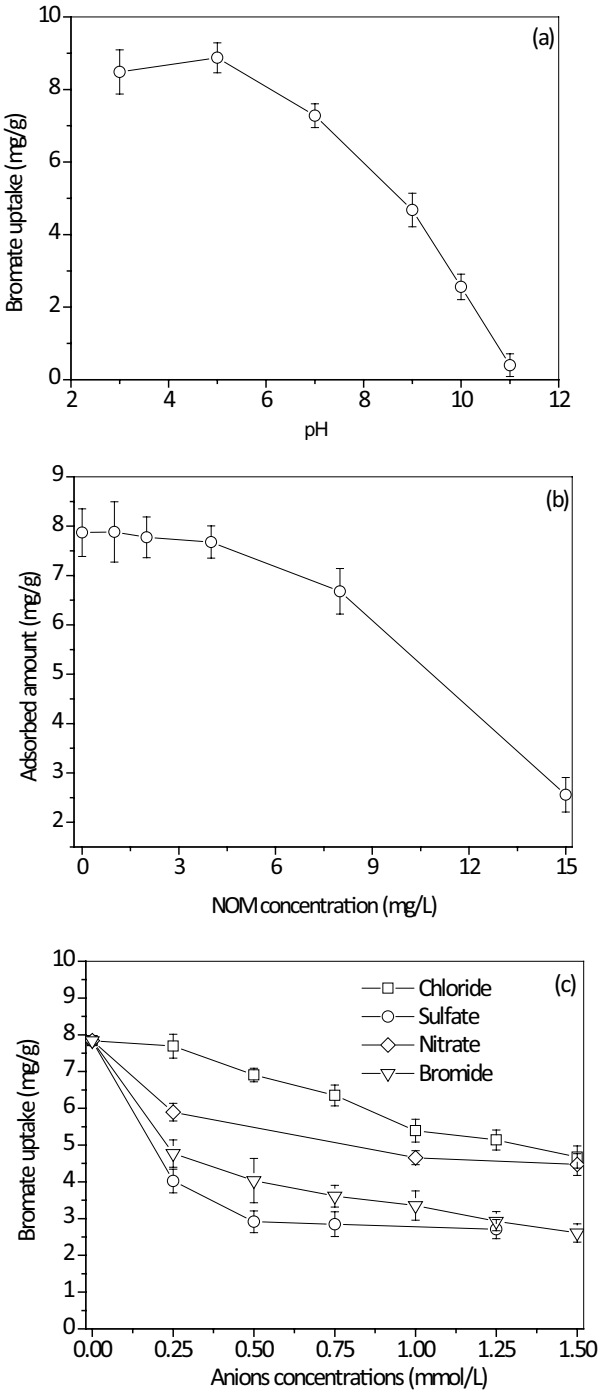

Fig. 8. Effect of pH (a), NOM (b), and competing anions (c) on bromate adsorption

3.6. Recycling performance

The reusability of the α-FeOOH bentonite was evaluated by regenerating them via the method of alkalinity eluting. The used bentonite was immersed into a solution with pH of 12.0 and shaken for 24 h followed by 30 min of ultrasonication. The regenerated bentonite was then washed with distilled water and dried in an oven at 55°C and used for the next adsorption process under the same experimental conditions. It can be seen from Fig. 9 that the α-FeOOH bentonite was quite stable in repeat usage with about 15% decline of the adsorption ability after five times adsorption–regeneration cycle, indicating that the synthesized α-FeOOH bentonite possesses good stability and deserves further investigation for applications.

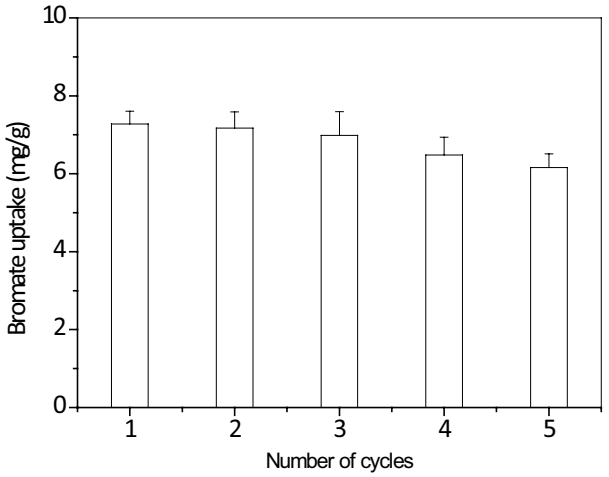

Fig. 9. Reusability of adsorbents for five consecutive reuses.

4. Conclusion

By comparing the adsorbility among Na-bentonite, Fe pillared bentonite, and α-FeOOH bentonite, α-FeOOH bentonite presented great superiority in bromate adsorption. Eight percent is the best loading ratio for α-FeOOH to bentonite, and the theoretic maximum adsorption capacity of the α-FeOOH at this loading ratio is about 19.56 mg/g. In the kinetic study, the bromate in solution was rapidly removed/adsorbed during the first 10 min, and the adsorption process tends to attain an equilibrium within 50 min. The adsorption process can be well-described by the pseudo-second-order kinetics. pH determines the adsorption process heavily, and the acidic pH condition is more favored in bromate uptake. The influences of competing anions and NOM were examined and both of them presented some negative effects on bromate adsorption.

Acknowledgments

The authors would like to acknowledge the financial support for this work provided by the Natural Science Foundation Project of Chongqing (cstc2017jcyjAX0173).

References

[1] K. Tyrovola, E. Diamadopoulos, Bromate formation during ozonation of groundwater, Desalination, 126 (2005) 201–209.
[2] X. Huang, N. Gao, Y. Deng, Bromate ion formation in dark chlorination and ultraviolet chlorination, J. Environ. Sci., 20 (2008) 246–251.
[3] Y. Kurokawa, A. Maekawa, M. Takahashi, Y. Hayashi, Toxicity and carcinogenicity of potassium bromated, Environ. Health Perspect., 87 (1990) 309–335.

[4] D. Liu, Z. Wang, Q. Zhu, F. Cui, Y. Shan, X. Liu, Drinking water toxicity study of the environmental contaminant-Bromate, Regul. Toxicol. Pharmacol., 73 (2015) 802–810.
[5] F. John, W. Mike, Approaches to determining regulatory values for carcinogens, Toxicology, 221 (2006) 149–153.
[6] L. Ding, Q. Li, C. Hao, R. Tang, H. Xu, X. Xie, J. Zhai, Electrocatalytic reduction of bromate ion using a polyaniline-modified electrode: an efficient and green technology for the removal of BrO_3^- in aqueous solutions, Electrochim. Acta, 55 (2010) 8471–8475.
[7] L. Xie, C. Shang, Effects of copper and palladium on the reduction of bromate by Fe(0), Chemosphere, 64 (2006) 919–930.
[8] K.A. Lin, C.H. Lin, Enhanced reductive removal of bromate using acid-washed zero-valent iron in the presence of oxalic acid, Chem. Eng. J., 325 (2017) 144–150.
[9] J.A. Wiśniewski, M. Kabsch-Korbutowicz, Bromate removal in the ion-exchange process, Desalination, 261 (2010) 197–201.
[10] N.I. Chubar, V.F. Samanidou, V.S. Kouts, G.G. Gallios, V.A. Kanibolotsky, V.V. Strelko, I.Z. Zhuravlev, Adsorption of fluoride, chloride, bromide, and bromate ions on a novel ion exchanger, J. Colloid Interface Sci., 291 (2005) 67–74.
[11] K. Listiarini, J.T. Tor, D.D. Sun, J.O. Leckie, Hybrid coagulation–nanofiltration membrane for removal of bromate and humic acid in water, J. Membr. Sci., 365 (2010) 154–159.
[12] P.N. Dave, S. Sharma, N. Subrahmanyam, Kinetics and thermodynamics of copper ions removal from wastewater by use of bentonite, J. Indian Chem. Soc., 89 (2012) 947–954.
[13] Z. Yang, Q. Xiao, B. Chen, L. Zhang, H. Zhang, X. Niu, S. Zhou, Perchlorate adsorption from aqueous solution on inorganic-pillared bentonites, Chem. Eng. J., 223 (2013) 31–39.
[14] O. Duman, S. Tunç, T. Gürkan Polat, Adsorptive removal of triarylmethane dye (Basic Red 9) from aqueous solution by sepiolite as effective and low-cost adsorbent, Microporous Mesoporous Mater., 210 (2015) 176–184.
[15] F. Tomul, Effect of ultrasound on the structural and textural properties of copper-impregnated cerium-modified zirconium-pillared bentonite, Appl. Surf. Sci., 258 (2011) 1836–1848.
[16] S. Barakan, V. Aghazadeh, Synthesis and characterization of hierarchical porous clay heterostructure from Al, Fe-pillared nano-bentonite using microwave and ultrasonic techniques, Microporous Mesoporous Mater., 278 (2019) 138–148.
[17] F. Tomul, F.T. Basoglu, H. Canbay, Determination of adsorptive and catalytic properties of copper, silver and iron contain titanium-pillared bentonite for the removal bisphenol A from aqueous solution, Appl. Surf. Sci., 360 (2016) 579–593.
[18] P. Kumararaja, S. Suvana, R. Saraswathy, N. Lalitha, M. Muralidhar, Mitigation of eutrophication through phosphate removal by aluminium pillared bentonite from aquaculture discharge water, Ocean Coastal Manage., 182 (2019) 104951, doi: 10.1016/j.ocecoaman.2019.104951.
[19] L. Perelomov, B. Sarkar, M.M. Rahman, A. Goryacheva, R. Naidu, Uptake of lead by Na-exchanged and Al-pillared bentonite in the presence of organic acids with different functional groups, Appl. Clay Sci., 119 (2016) 417–423.
[20] F. Tomul, Adsorption and catalytic properties of Fe/Cr-pillared bentonites, Chem. Eng. J., 185–186 (2012) 380–390.
[21] Y. Hao, L. Yan, H. Yu, K. Yang, S. Yu, R. Shan, B. Du, Comparative study on adsorption of basic and acid dyes by hydroxy-aluminum pillared bentonite, J. Mol. Liq., 199 (2014) 202–207.
[22] S. Tunç, O. Duman, B. Kancı, Rheological measurements of Na-bentonite and sepiolite particles in the presence of tetradecyltrimethylammonium bromide, sodium tetradecyl sulfonate and Brij 30 surfactants, Colloids Surf., A, 398 (2012) 37–47.
[23] L.G. Yan, Y.Y. Xu, H.Q. Yu, X.D. Xin, Q. Wei, B. Du, Adsorption of phosphate from aqueous solution by hydroxy-aluminum, hydroxy-iron and hydroxy-iron–aluminum pillared bentonites, J. Hazard. Mater., 179 (2010) 244–250.
[24] G. Murambasvina, C. Mahamadi, Effective fluoride adsorption using water hyacinth beads doped with hydrous oxides of aluminium and iron, Groundwater Sustainable Dev., 10 (2020) 100302, doi: 10.1016/j.gsd.2019.100302.
[25] E. Kumar, A. Bhatnagar, M. Ji, W. Jung, S.H. Lee, S.J. Kim, G. Lee, H. Song, J.Y. Choi, J.S. Yang, B.H. Jeon, Defluoridation from aqueous solutions by granular ferric hydroxide (GFH), Water Res., 43 (2009) 490–498.
[26] P.S. Kumar, R.Q. Flores, C. Sjöstedt, L. Önnby, Arsenic adsorption by iron–aluminium hydroxide coated onto macroporous supports: insights from X-ray absorption spectroscopy and comparison with granular ferric hydroxides, J. Hazard. Mater., 302 (2016) 166–174.
[27] A. Genz, B. Baumgarten, M. Goernitz, M. Jekel, NOM removal by adsorption onto granular ferric hydroxide: equilibrium, kinetics, filter and regeneration studies, Water Res., 42 (2008) 238–248.
[28] X.H. Guang, J.M. Wang, C.C. Chusuei, Removal of arsenic from water using granular ferric hydroxide: macroscopic and microscopic studies, J. Hazard. Mater., 156 (2008) 178–185.
[29] A. Bhatnagar, Y.H. Choi, Y.J. Yoon, Y. Shin, B.H. Jeon, J.W. Kang, Bromate removal from water by granular ferric hydroxide (GFH), J. Hazard. Mater., 170 (2009) 134–140.
[30] J. Chen, L. Zhu, Comparative study of catalytic activity of different Fe-pillared bentonites in the presence of UV light and H_2O_2, Sep. Purif. Technol., 67 (2009) 282–288.
[31] L. Lei, X. Li, X. Zhang, Ammonium removal from aqueous solutions using microwave-treated natural Chinese zeolite, Sep. Purif. Technol., 58 (2008) 359–366.
[32] M. Badruzzaman, P. Westerhoff, D.R.U. Knappe, Intraparticle diffusion and adsorption of arsenate onto granular ferric hydroxide (GFH), Water Res., 38 (2004) 4002–4012.
[33] O. Duman, C. Özcan, T.G. Polat, S. Tunç, Carbon nanotube-based magnetic and non-magnetic adsorbents for the high-efficiency removal of diquat dibromide herbicide from water: OMWCNT, OMWCNT-Fe_3O_4 and OMWCNT-κ-carrageenan-Fe_3O_4 nanocomposites, Environ. Pollut., 244 (2019) 723–732.
[34] O. Duman, S. Tunç, T.G. Polat, Determination of adsorptive properties of expanded vermiculite for the removal of C.I. Basic Red 9 from aqueous solution: kinetic, isotherm and thermodynamic studies, Appl. Clay Sci., 109–110 (2015) 22–32.
[35] E. Ayranci, O. Duman, Structural effects on the interactions of benzene and naphthalene sulfonates with activated carbon cloth during adsorption from aqueous solutions, Chem. Eng. J., 156 (2010) 70–76.
[36] T. Hiemstra, W.H. Van Riemsdijk, Fluoride adsorption on goethite in relation to different types of surface sites, J. Colloid Interface Sci., 225 (2000) 94–104.

Supplementary information

Table S1
Textural property of bentonites with different ferric supporting ratios

	Supporting ratios	BET specific surface area (m^2/g)	Total pore volume (cm^3/g)	Average pore size (nm)
α-FeOOH-bentonite	2%	57.2	0.15	4.23
	5%	86.3	0.19	4.81
	8%	113.2	0.23	5.23
	15%	68.3	0.16	4.68

Table S1 presents the textural property of different bentonites with different ferric supporting ratios, according to their N_2 adsorption/desorption isotherms. It can be seen from the Table S1, there is a significant increase of the porous structure, with the increasing of the specific surface area from 57.2 m^2/g at the supporting ratio of 2% to 113.2 m^2/g at 8%. Further increase of the supporting ratio to 15% brought a significant decrease of the specific surface area to 68.3 m^2/g. The total pore volume, as well as the average pore size, also present similar trend with the increase of the supporting ratios.